Using Self-Assembly To Prepare Multifunctional Diblock Copolymers Containing Azopyridine Moiety

Li Cui,[†] Smail Dahmane,[†] Xia Tong,[†] Lei Zhu,[‡] and Yue Zhao*,[†]

Département de chimie, Université de Sherbrooke, Sherbrooke, Québec, Canada J1K 2R1, and Centre de recherche en science et ingénierie des macromolécules (CERSIM), Université Laval, Québec, Canada G1K 7P4, and Department of Chemical Engineering, University of Connecticut, Storrs, Connecticut 06269-3136

Received December 21, 2004; Revised Manuscript Received January 11, 2005

ABSTRACT: Diblock copolymers composed of polystyrene (PS) and a polymethacrylate containing an azopyridine side group (PAzPy) were synthesized using atom transfer radical polymerization for the first time. While conserving the photoactivity related to the trans−cis photoisomerization of azo dyes, the azopyridine moiety made possible the easy use of self-assembly to add new functionalities to the PAzPy block, leading to multifunctional diblock copolymers. On one hand, three carboxylic acids (one aliphatic, one aromatic, and one chiral acid) were complexed with azopyridine moieties through hydrogen bonding which transformed the amorphous PAzPy block into a liquid crystalline (LC) block. Self-assembly-induced LC phases, dependent on the nature of the acid used, could enhance the photoinduced orientation of azopyridine moieties. On the other hand, zinc−tetraphenylporphyrin (ZnTPP) was linked to azopyridine through coordination interaction between the metal and pyridyl group, showing effective loading of metal−porphyrine inside microdomains of the PAzPy block. The complexation with ZnTPP made the PAzPy block become both photoactive and electroactive. This work demonstrates the interest of the strategy of exploiting self-assembly through the use of azopyridine-containing block copolymers.

Introduction

Block copolymers can self-assemble into various nanostructures both in solution and in the solid state. Of the many approaches that allow preparing block copolymers of novel chemical structures and properties, the use of self-assembly to transform the building blocks is attractive. For example, Ober, Thomas, and co-workers were able to introduce the liquid crystallinity in an initially amorphous diblock copolymer of polystyrene-*b*-poly(acrylic acid) (PS-*b*-PAA) through hydrogen bonding between an imidazole-terminated mesogen and the carboxylic acid groups of PAA.[1] They showed that orientational switching of both mesogens and microdomains could be achieved using an ac electric field partly due to the dynamic nature (temperature-dependent dissociation and formation) of H-bonds.[1] It can be envisioned that self-assembly can also be a powerful tool in the search of block copolymers that possess multiple functionalities. Multifunctional block copolymers may offer new possibilities in the design of advanced materials. For instance, using atom transfer radical polymerization (ATRP), we prepared different photoactive and liquid crystalline block copolymers.[2−5] The functionalities of photoactivity and liquid crystallinity come from the use of an azobenzene-containing side-chain liquid crystalline polymer (Azo-SCLCP) in the structures of block copolymers. By design, the reversible trans−cis photoisomerization of the azobenzene chromophore as well as the related photoalignment and photochemical phase transition in Azo-SCLCPs gave rise to new properties for these block copolymers. In one case, thermoplastic elastomers with Azo-SCLCP microdomains acting as physical cross-links were obtained, and the coupling between liquid crystallinity, elasticity, and photoactivity resulted in unique features.[4] In another case, the combined amphiphilicity and photoactivity of Azo-SCLCP-based diblock copolymers led to light-induced reversible changes in micellar aggregates formed in solution, including core−shell micelles and vesicles.[5]

The purpose of the present study is to explore the use of self-assembly to prepare multifunctional block copolymers. Recently, we described an easy approach that allows the exploitation of self-assembly in azo polymers.[6] The strategy is to use azopyridine-based side-chain polymers that conserve the photoactivity of azobenzene polymers while providing the capability for self-assembly through the pyridyl group. We showed that an amorphous polymethacrylate with azopyridine in its side chain was readily converted to photoactive LCP through H-bonding between azopyridine groups and a series of commercially available carboxylic acids including the acetic acid.[6] In this paper, we report on the synthesis of the first example of diblock copolymers containing an azopyridine side-chain polymer (PAzPy) and demonstrate the use of self-assembly to transform the amorphous diblock copolymer into either photoactive liquid crystalline or photo- and redox-active diblock copolymer. Figure 1 shows the chemical structures of the amorphous diblock copolymer PS-*b*-PAzPy as well as the three carboxylic acids (aliphatic, aromatic, and chiral) and zinc−tetraphenylporphyrin (ZnTPP) used to complex with the azopyridine moiety through H bonding or metal coordination.

Experimental Section

1. Synthesis. a. Materials. THF was refluxed with sodium and distilled. Styrene was distilled with 2,6-di(*tert*-butyl-4-methyl)phenol as inhibitor before use. The synthesis of the monomer for PAzPy, 6-[4-(4-pyridyazo)phenoxy]hexyl methacrylates, was already reported.[6] Among the three acids used for self-assembly, 4-(decyloxy)benzoic acid (10OBA) was prepared following a literature method,[7] and the synthesis of

[†] Université de Sherbrooke and Université Laval.
[‡] University of Connecticut.
* Corresponding author: e-mail yue.zhao@usherbrooke.ca.

10.1021/ma047364m CCC: $30.25
Published on Web 02/11/2005

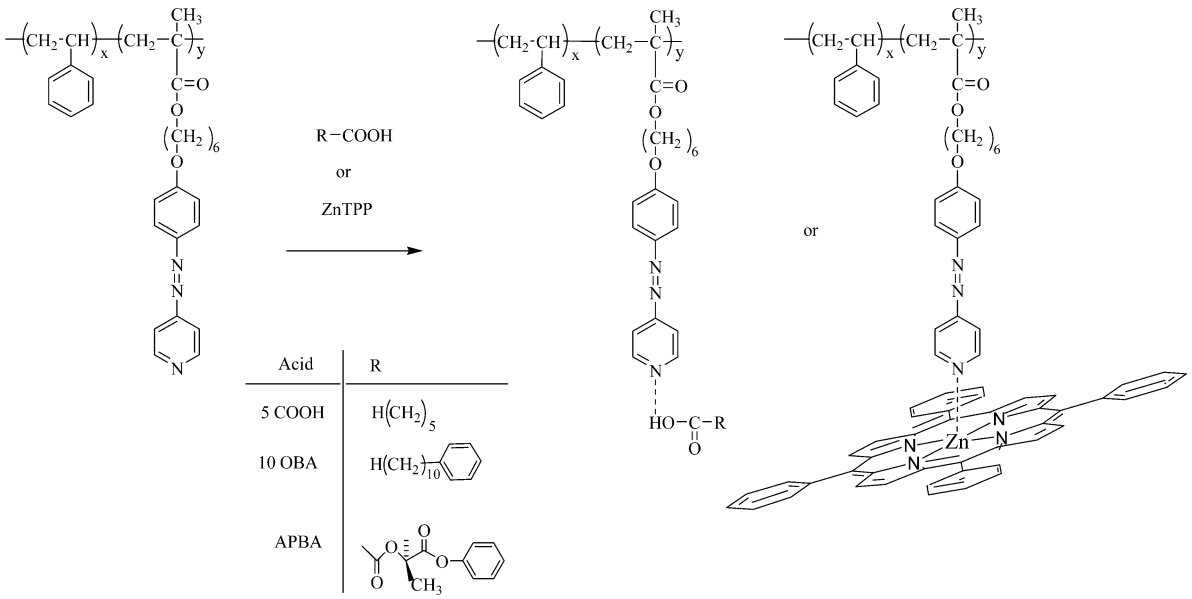

Figure 1. Chemical structure of the PS-*b*-PAzPy diblock copolymer. Chemical structures and acronyms of the acids and zinc−tetraphenylporphyrin used to complex with the PAzPy block through hydrogen-bonding and coordination interaction, respectively, are also shown.

4-[(*S*)-2-Acetoxypropionoyl]benzoic acid (APBA) is reported below. Regarding hexanoic acid (5COOH) and ZnTPP, the samples were purchased from Aldrich. Tris[2-(dimethylamino)-ethyl]amine used for ATRP was also synthesized according to the literature.[8] The other commercially available chemicals (Aldrich) were used without further purification.

b. Preparation of 4-[(*S*)-2-Acetoxypropionoyl]benzoic Acid. 4-Hydroxybenzoic acid (0.64 g, 5 mmol) was dissolved in 5 mL of dry THF, to which 78 mL of triethyleneamine (5.5 mmol) was added. A solution of (*S*)-(−)-2-acetoxypropionoyl chloride (0.91 g, 5.5 mmol) in 3 mL of THF was then added dropwise at room temperature. The reaction mixture was stirred overnight. Afterward, the mixture was poured into 50 mL of water and extracted with chloroform. The chloroform solution was dried over Na_2SO_4 and evaporated. The residue was dissolved in ethyl acetate and separated by a silica gel column chromatograph with ethyl acetate as eluent; 0.76 g of white powder (57%) was obtained. MS (*m/e*): 252 (M^+). ^{1}H NMR (300 MHz, $CDCl_3$) δ: 1.57 (d, 3H, CH_3), 2.20 (d, 3H, CH_3), 5.26 (q, 1H, CH), 7.24 (d, 2H, aromatic), 8.15 (d, 2H, aromatic).

c. Synthesis of Azopyridine Block Copolymers. Diblock copolymers of PS-*b*-PAzPy were prepared using ATRP. Since the same procedure as for the synthesis of a diblock copolymer composed of PS and an Azo-SCLCP,[2] referred to as PS-*b*-PAzo, was utilized, details will not be repeated here. In essence, PS macroinitiator was first prepared and then used to polymerize the azopyridine monomer. There was however one difference in the choice of the catalyst system for ATRP. Because of the coordination property of the pyridyl group, the azopyridine monomer may compete with the growing polymer by interacting with the catalyst to bind the copper. To minimize this problem, tris[2-(dimethylamino)ethyl]amine (Me6TREN) was utilized for PS-*b*-PAzPy instead of pentamethyldiethylenetriamine (PMDETA) used in the case of PS-*b*-PAzo.[2] Me6TREN is a strong ligand due to its branched multidentate character and was successfully used to polymerize pyridine-containing monomers,[9,10] Prior to the preparation of PS-*b*-PAzPy diblock copolymers, the effectiveness of the catalyst was confirmed by polymerizing the azopyridine monomer with copper bromide complexed with Me_6TREN and ethyl 2-bromoisobutyrate as initiator, which resulted in the homopolymer PAzPy (Table 1). Then, the same catalyst system was used with the PS−Br macroinitiator to polymerize the azopyridine monomer leading to PS-*b*-PAzPy diblock copolymers. It was found that the conversion of azopyridine monomer was low (~40−50%) even with prolonged reaction time. The characteristics of three diblock copolymers used in this study are shown in Table 1.

Table 1. Characteristics of the Polymers

polymer	azopyridine block content (wt %)[a]	M_n (NMR)	M_n (GPC)	M_w/M_n (GPC)
PS-Br	0		14 500	1.25
P1	8.8	15 900	16 600	1.25
P2	22.0	18 600	18 900	1.29
P3	44.4	26 100	24 500	1.34
PAzPy	100		20 500	1.32

[a] Calculated from NMR data.

2. Preparation of Complexes. In all cases, the diblock copolymer and an acid or ZnTPP were dissolved in THF to make a clear solution. Then, most of the solvent was evaporated slowly under ambient conditions, which was followed by drying in a vacuum oven at 60 °C for several hours. The complexation through H bonding or coordination occurred during the solvent evaporation. The complexes of PS-*b*-PAzPy/acid had the equal amount for the pyridyl and carboxylic acid groups (1:1 molar ratio). In the complexes of PS-*b*-PAzPy/ZnTPP, the molar ratio of Zn to pyridyl groups was chosen to be 0.6. This choice was based on our studies of the homopolymer PAzPy complexed with ZnTPP, which found thorough complexation of ZnTPP at this ratio and significant changes in polymer properties such as T_g.

3. Characterizations. The synthesized diblock copolymers and their complexes with acids and ZnTPP were characterized using a number of techniques. ^{1}H NMR spectra were recorded on a Bruke spectrometer (300 MHz, AC 300). Molecular weights and polydispersities were measured by gel permeation chromatography (GPC) using a Waters system equipped with a refractive index and a photodiode array detector; THF was used as eluent (elution rate, 0.5 mL/min), and polystyrene standards were used for calibration. A Perkin-Elmer DSC-7 differential scanning calorimeter was used to investigate the thermal phase transitions with a heating and cooling rate of 10 °C/min. Infrared and UV−vis spectra were recorded on a Bomem-MB102 FTIR spectrometer and a Hewlett-Packard 8452A diode array spectrophotometer, respectively. Textures were observed with a Leitz DMR-P polarizing microscope equipped with an Instec hot stage. For the complexes of PS-*b*-PAzPy/acid, X-ray scattering measurements were conducted on a Bruker diffractometer with a two-dimensional (2D) position-sensitive wire-grid detector (Bruker AXS). On the other hand, for the detection of microphase separation in the diblock copolymers, the 2D small-angle X-ray scattering

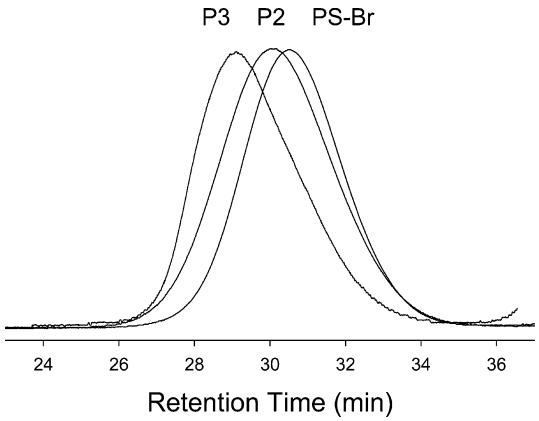

Figure 2. GPC curves of PS-Br macroinitiator and two diblock copolymers.

(SAXS) experiment was performed at the synchrotron X-ray beamline X27C in the National Synchrotron Light Source, Brookhaven National Laboratory. The wavelength of the X-ray beam was 0.154 nm. The beam center was calibrated using silver behenate with the primary reflection peak at 1.076 nm^{-1}. Typical data acquisition time was 1 min. 2D images were obtained using Fuji imaging plates equipped with a Fuji BAS-2500 scanner. One-dimensional (1D) SAXS curves were obtained by integration of the corresponding 2D SAXS patterns. TEM experiments were performed on a Philips EM300 at an accelerating voltage of 80 kV. Thin sections with a thickness of ~75 nm were obtained with a diamond knife at room temperature on a Leica Ultracut UCT microtome. The thin sections, floating on a water boat, were then collected onto 400 mesh TEM grids and stained in RuO_4 vapor at room temperature for 15 min. Irradiation of samples was performed using an UV and visible spot curing system (Novacure 2100) combined with interference filters (10 nm bandwidth, Oriel). UV light at $\lambda = 365$ nm and visible light at $\lambda = 440$ nm were used for irradiations. Cyclic voltammetry (CV) was performed on a potentiostat/galvanostat (Princeton Applied Research, model 263A) controlled by an external PC (Research Electrochemistry Software 4.23), to which was connected a three-electrode system. The experiment was conducted in an acetonitrile solution with 0.1 M tetrabutylammonium perchlorate (TBAP), scan rate being 100 mV/s. In the case of polymers dissolved in solution, about 1 mL of a 10% CH_2Cl_2 solution was added in 10 mL of the acetonitrile solution, and the working electrode was a vitreous carbon disk (5 mm diameter), which was polished with an aqueous alumina slurry and sonicated in distilled water and rinsed with acetone after each polishing step. For polymers in the solid state, thin films (about 1 μm thick) were spin-coated from CH_2Cl_2 solution on indium−tin oxide (ITO) coated glass plate, with ITO serving as the working electrode, and dried in a vacuum for 12 h at room temperature. For both polymer solution and films, a Pt wire was used as the counter electrode, and a saturated calomel electrode (SCE) was used as the reference, which was separated from the test solution by a fritted supporting electrolyte/solvent bridge. All solutions were degassed with nitrogen for 15 min prior to electrochemical measurements.

Results and Discussion

1. Characterization of Diblock Copolymers. The controlled growing of the PAzPy block from the PS−Br macroinitiator can be seen from Figure 2 where the GPC curves of PS-Br and two PS-*b*-PAzPy diblock copolymer (P2 and P3 in Table 1) are compared. Despite a small tailing effect on the side of high retention time for the samples, which may be due to the interaction of the strong polar pyridine group with the GPC columns when using THF as eluent,[10] the block copolymer have only a slightly increased polydispersity as compared to the PS-Br macroinitiator. Figure 3 shows the ^1H NMR spectrum of P2. From the peak assignment the composition of PS-*b*-PAzPy could be determined, and in conjunction with the GPC value for the PS block, an NMR-based average molecular weight could be estimated. Table 1 summarizes the characteristics of PS-Br, PAzPy, and three obtained PS-*b*-PAzPy diblock copolymers of different compositions. From the same PS-Br macroinitiator, the polydispersity of diblock copolymers increases, though slightly, with lengthening the length of the azopyridine polymer block.

The microphase separation in the PS-*b*-PAzPy diblock copolymer is clearly revealed by the DSC measurement. Figure 4 shows the second heating curves of all samples. Like the PS-Br macroinitiator, PAzPy is an amorphous polymer but displays a lower T_g around 40 °C. For diblock copolymers, T_g's of the two polymers are well visible, and their relative prominence varies with the composition of the diblock copolymer, except for P1 for which T_g of the PAzPy block is not clearly discernible due to the low content of 10%. It is also noticeable that T_g of the PS block is slightly lower than that of PS-Br, which is indicative of some interfacial mixing of the two blocks. The microphase separation in the samples has also been studied by SAXS, and the corresponding Lorentz-corrected profiles are shown in Figure 5, where I is the relative scattering intensity and q is the scattering vector ($q = 4\pi \sin\theta/\lambda$, where λ is the X-ray beam wavelength and θ is the half scattering angle). With increasing the overall molecular weight in the sample, the average d spacing increases. The microphase separation can be determined from the full width at half-maximum (fwhm). For the P1 sample, the fwhm is 0.19 nm^{-1}, and thus a density-fluctuation-induced disordered phase can be identified. For the P2 and P3 samples, no distinct higher order reflections are observable, except that there is a broad hump in the SAXS profile for P3. The fwhm values for P2 and P3 are 0.074 and 0.098 nm^{-1}, respectively, which are slightly higher than those reported for microphase-separated block copolymers (e.g., 0.03 nm^{-1} for a lamellar PS-*b*-PEO sample).[11] We thus conclude that the P2 and P3 samples should be microphase separated, as revealed by the two distinct T_g's in the DSC measurements in Figure 4. We speculate that due to relatively broad molecular weight distribution in these samples, the grain sizes may be small, and thus slightly broader fwhm's are observed. To determine the microphase-separated structure, a TEM study has been carried out. Figure 6 shows an example of the bright-field TEM micrographs for P2. In the top right of the micrograph, one can see that the grain size is indeed relatively small (only 100−200 nm). The packing of the azopyridine cylinders does not possess a well-defined hexagonal lattice, as judged from the top left of the micrograph. These observations may explain the absence of the higher order reflections in the SAXS profile for P2. We were unable to determine the morphology of P3 using TEM though its weight fraction of PAzPy (Table 1) implies lamellar microdomains for the azopyridine polymer block. As a whole, however, the characterization results confirm the microphase separation in P2 and P3. Finally, note that similar to the PAzPy homopolymer,[6] azopyridine groups in the PAzPy block of the copolymers display reversible trans−cis photoisomerization on alternating UV and visible light irradiation.

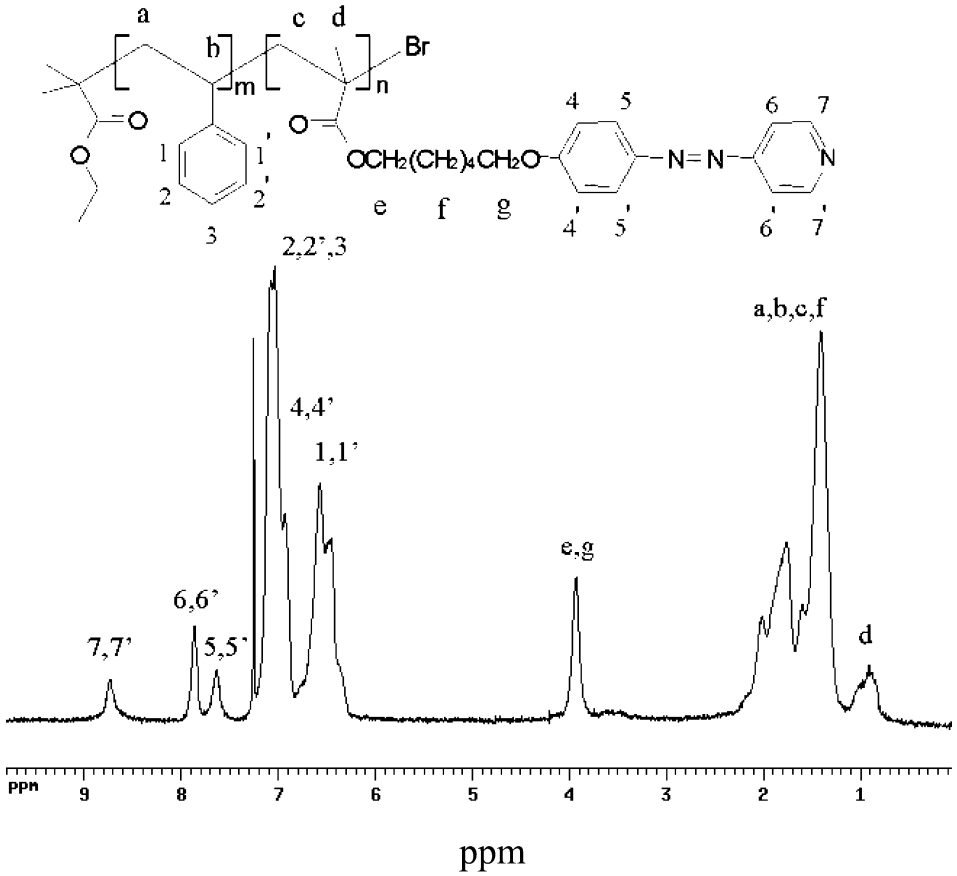

Figure 3. ^{1}H NMR spectrum of a PS-*b*-PAzPy diblock copolymer (P2 sample).

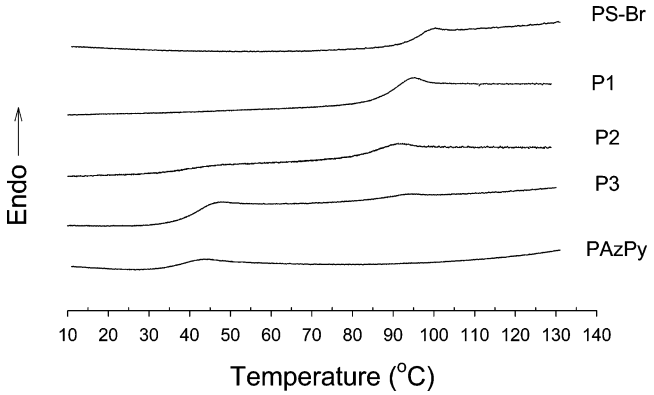

Figure 4. DSC heating curves (second scan) of PS-Br, three diblock copolymers (P1−P3 samples), and a sample of PAzPy homopolymer.

2. Photoactive and Liquid Crystalline Diblock Copolymers. To transform the amorphous photoactive block of PAzPy in PS-*b*-PAzPy into liquid crystalline photoactive block through self-assembly, three different carboxylic acids (see structures and acronyms in Figure 1) were used to complex with the block copolymers P2 and P3 through H bonding between the azopyridine and acid groups. Polymer self-assembly through H bonding between pyridyl and carboxylic acid groups was well-known.[12] Summarized in Table 2 are the phase transition temperatures measured from DSC on second heating scan for the complexes of block copolymers and, for comparison, the homopolymer PAzPy as well. The mesophase identification was supported by X-ray diffraction and polarizing microscope (POM) observations

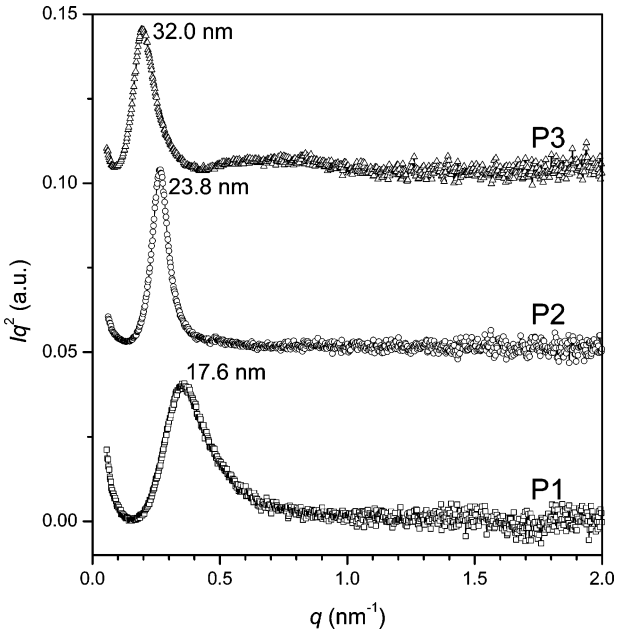

Figure 5. 1D Lorentz-corrected SAXS profiles for three diblock copolymers (P1−P3 samples). The *d* spacing calculated from the peak position is listed for each sample.

as will be discussed later. Figure 7 shows the DSC heating and cooling curves (second scan) of P2 and P3 complexed with the three acids. In the case of 5COOH, knowing that the pure aliphatic acid is liquid under ambient conditions and has a boiling temperature of 204 °C, the endothermic peaks on heating and exothermic peaks on cooling indicate clearly the formation of LC

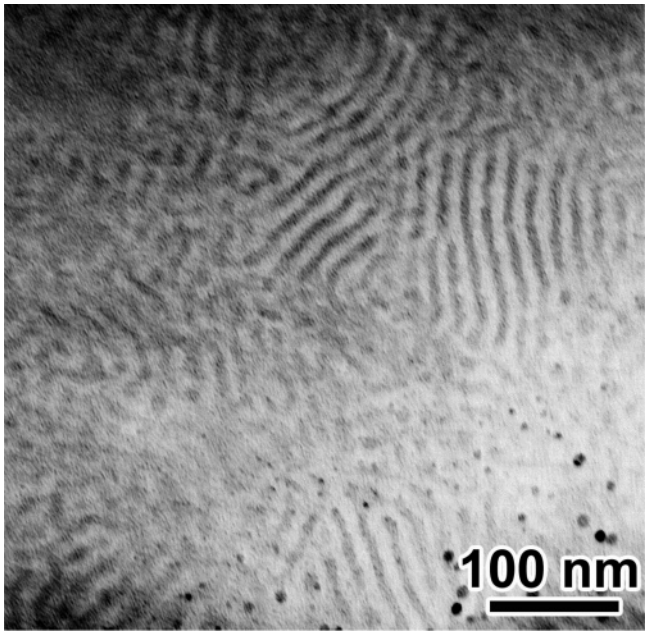

Figure 6. TEM image of P2 sample.

phases in the complexes. In the case 10OBA, the complex with P2 shows a LC isotropic clearing temperature of 120 °C, whereas the P3 complex displays a broad mesophase transition peak at about 125 °C. For complexes with APBA, on the first heating scan, two endothermic peaks at about 93 and 116 °C for the P3 complex and one peak at 110 °C for the P2 complex were observed (curves not shown). However, on second heating scan, only a very broad peak can barely be noticed around 90 °C (LC phase confirmed by POM). This observation seems to indicate that the LC phases formed in the complexes with APBA were not stable on heating into the isotropic phase. But the absence of the melting peak of pure APBA (144 °C) even on the second heating scan suggests that there were no phase separation in the isotropic phase leading to the crystallization of APBA. For all the three acids, the phase transition peaks of the P3 complex are shifted to higher temperatures as compared with the P2 complex, which reflects the influence of the microdomain morphology of the PAzPy block on the thermal stability of the LC phases. Since P3 has a higher content of the PAzPy block, the restriction imposed on azopyridine mesogens could be less severe than in P2 for which azopyridine mesogens are located inside cylindrical microdomains. Comparing the results of the block copolymers with those obtained with the homopolymer PAzPy, the effect of the block length seems unclear for the complexes with 5COOH. However, it becomes significant for the complexes with the larger, aromatic acids of 10OBA and APBA. The PAzPy/10OBA complex has a clearing temperature of 133 °C,[6] which is about 10 °C higher than those of the block copolymer complexes. In the case of APBA, the complex with PAzPy showed prominent mesophase transition endothermic peaks around 112 °C on the second heating scan, and the X-ray scattering measurement found small-angle diffractions corresponding to a monolayer smectic phase, which differs from the block copolymer complexes showing no smectic phase. These results suggest that the microdomain morphologies in block copolymers affect more severely the LC phases of the LCP block containing larger H-bonded mesogenic side groups. Another indication for the LC phases formed in the complexes with P2 and P3 is the small supercooling for all the transition peaks in Figure 7. Such small supercooling is characteristic of LC phases, in contrast with a crystalline phase that should display much more important supercooling at the used cooling rate of 10 °C/min.

X-ray scattering measurements were performed to get more information on the LC phases induced by self-assembly. Similar results were obtained for both P2 and P3 complexed with 5COOH. As can be seen from the diffraction patterns of the P2 complex on cooling from the isotropic phase (80 °C), in Figure 8, the formation of a monolayer smectic phase is suggested by the small-angle diffraction at $2\theta \sim 3.15°$, which corresponds to a layer spacing of 28 Å that is very close to the total length of the side chain (PAzoPy + 5COOH), and the wide-angle diffuse halo at $2\theta \sim 19°$, which is associated with the liquidlike two-dimensional organization of the mesogens within the layer. Combined with the DSC measurement revealing the superimposition of two peaks (Figure 7), the other mesophase of very narrow temperature range (on the high-temperature side) should be nematic. For the complexes with 10OBA, Figure 9 shows the results of the P3 complex on cooling from the isotropic phase. Essentially, the prominent low-angle diffraction indicates a smectic phase. The peak maximum of $2\theta \sim 2.1°$ corresponds to a layer spacing of 41 Å that also is very close to the total length of the H-bonded side chain, suggesting a monolayer smectic phase. Interestingly, the P2/10OBA complex displays no small-angle diffraction (patterns not shown), which suggests a nematic phase for this complex. Again, different microdomain morphologies for P2 and P3 may be the cause. The H-bonded mesogenic core with 10OBA is much (about 13 Å) longer than that with 5COOH. This may make the organization of mesogens more sensitive to the confinement effect of the microdomains of the PAzPy block. It appears that the smectic layering of long mesogens could not be developed inside the cylindrical microdomains of P2. Finally, for the complexes with the chiral acid APBA, no small-angle diffraction peak was observed, indicating the absence of any smectic phases.

On POM, all samples appeared birefringent, including P2 and P3 complexed with APBA. However, no clear textures could be observed for all complexes with P2, which is probably related to the cylindrical (smaller) microdomains of P2. For the complexes with P3, textures could be developed by annealing the sample for a certain time. Figure 10 shows examples of the polarizing micrographs of P3 complexed with the three acids. The textures of P3/5COOH and P3/10OBA are consistent with the smectic phases as reveled by X-ray diffraction. The batonnet texture of P3/5COOH indicates a smectic A phase, while the apparently broken focal conic texture suggests a smectic C phase in P3/10OBA. For the sample of P3/APBA, fingerprint texture can be noticed in some areas, which suggests the formation of a cholesteric phase through H bonding the chiral acid to the azopyridine group. In all complexes, the formation of strong H bonds between the pyridine and acid groups was confirmed by infrared spectroscopy. Figure 11 shows the spectra at room temperature of P3 complexed with the three acids. The characteristic H-bonded O−H bands near 2500 and 1940 cm^{-1} appeared in all the samples.[13,14]

Table 2. Phase Transition Temperatures (°C) of the Complexes[a]

acronym	pure acid	P2/acid	P3/acid	PAzPy/acid[b]
5COOH	C-3I	g38S71I	g42S77I	g44S72I
10OBA	$C_191C_2101S126N145I$	C72N120I	C84S125I	C92S133I
APBA	C144I	g45N90I	g40N94I	g34C90S112I

[a] g, glass transition; C, crystal; N, nematic; S, smectic; I, isotropic. [b] Data for 5COOH and 10OBA complexes previously reported in ref 6.

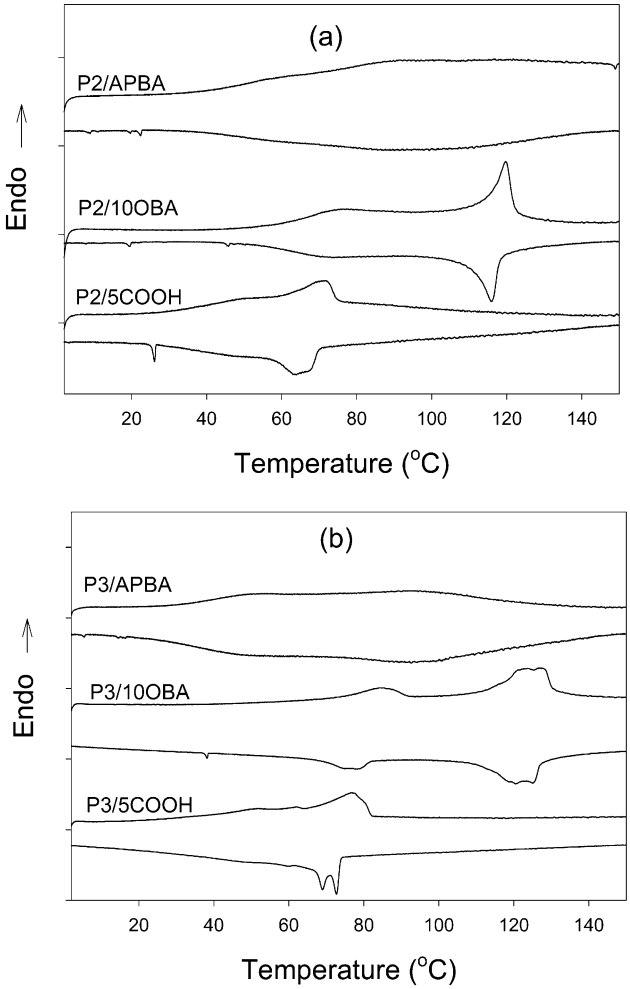

Figure 7. DSC heating and cooling curves (10 °C/min, second scan) for (a) P2 complexed with three acids and (b) P3 complexed with three acids.

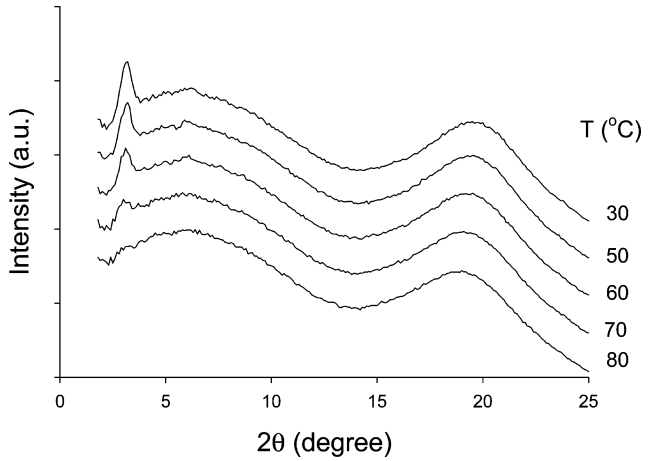

Figure 8. X-ray scattering patterns for the P2/5COOH complex on cooling from the isotropic phase (80 °C).

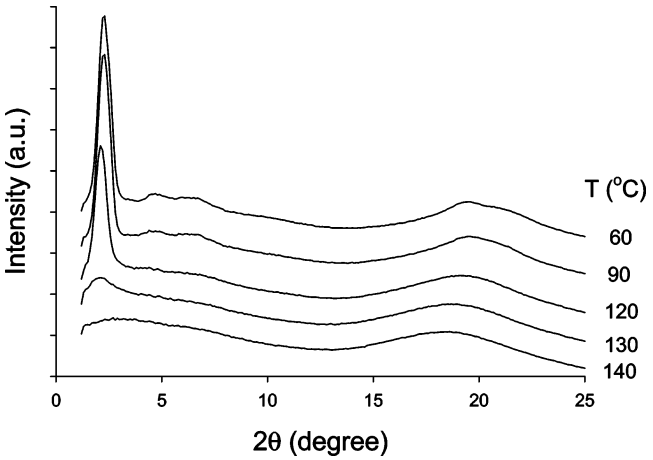

Figure 9. X-ray scattering patterns for the P3/10OBA complex on cooling from the isotropic phase (140 °C).

The above results indicate that in all cases the amorphous PAzPy block was readily converted into the LC block by linking the acid to the azopyridine moiety through H bonds (Figure 1). The acid provides the terminal group on the azopyridine moiety that is required for the formation of LC phases by azopyridine mesogens. As expected, the nature and chemical structure of the acid used affects the LC phases of the PAzPy block. The azopyridine moiety thus allows the use of self-assembly to transform the PS-*b*-PAzPy diblock copolymer to various LC and photoactive diblock copolymers. The reversible trans−cis photoisomerization of H-bonded azopyridine groups was observed. As an example, Figure 12 compares the photoinduced orientations of azopyridine moieties in thin films of P3 and P3/10OBA as measured from polarized UV−vis spectroscopy. In this experiment, the film was first irradiated with unpolarized UV light for 30 s (360 nm, 30 mW/cm^2) to reach the photostationary state rich in the cis conformation (>80%). Then, linearly polarized visible light (440 nm, 5 mW/cm^2) was applied to reconvert the contracted cis isomer to the rodlike trans isomer and, at the same time, to induce orientation of *trans*-azopyridine groups in the direction perpendicular to the polarization of the visible irradiation.[2] Shown in Figure 12 are the plots of order parameter of azopyridine vs time of the visible light irradiation. The order parameter S was measured from the dichroism of the maximum absorption of *trans*-azopyridine at 352 nm ($\pi-\pi^*$ transition) through $S = (A_{||} - A_{\perp})/(A_{||} + 2A_{\perp})$, where $A_{||}$ and $A_{\perp}$ are the absorbances with the spectrophotometer's beam polarized parallel and perpendicular, respectively, to the reference direction taken as the direction perpendicular to the polarization of the visible light irradiation. It is seen that the LC phase induced by self-assembly in P3/10OBA has a significant effect on the photoinduced orientation of azopyridine mesogens. For both samples, the orientation reaches a plateau value after about 2 min irradiation, which, however, is much higher for azopyridine mesogens H-bonded with the acid in the LC block of P3/10OBA than for azopyridine moieties in the

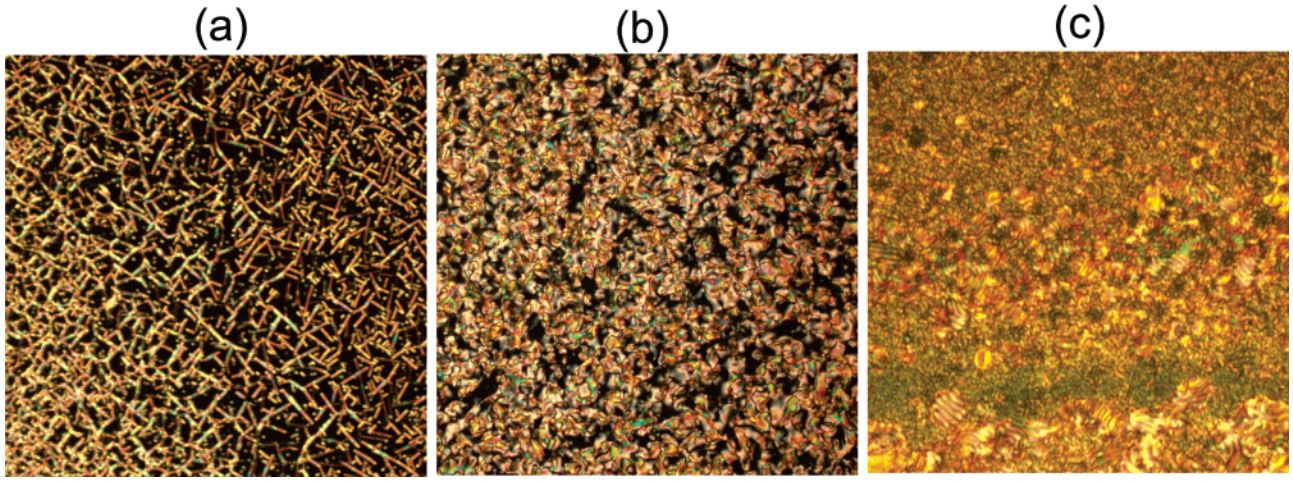

Figure 10. Polarizing optical micrographs for P3 complexed with (a) 5COOH (annealed at 70 °C), (b) 10OBA (annealed at 123 °C), and (c) APBA (annealed at 95 °C). Picture area: 430 μm × 430 μm.

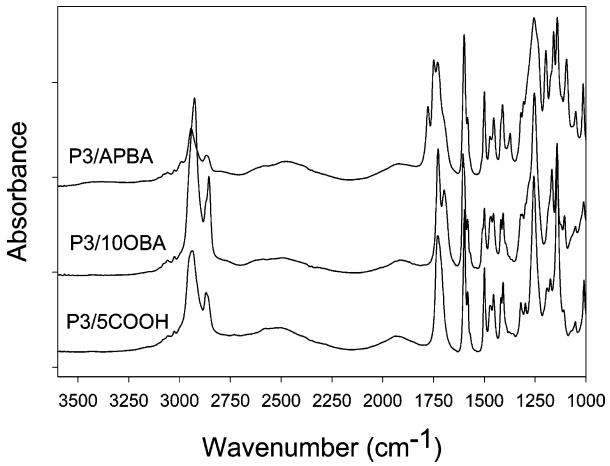

Figure 11. Infrared spectra at room temperature for P3 complexed with three acids.

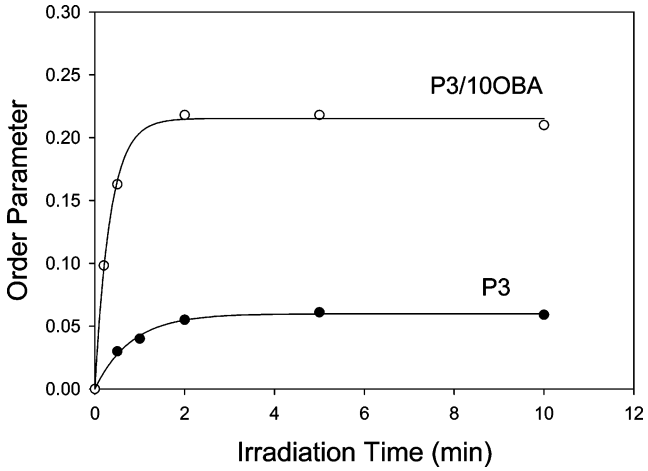

Figure 12. Order parameter of azopyridine mesogens vs irradiation time with linearly polarized visible light (440 nm) for P3 and the P3/10OBA complex. Films were treated with unpolarized UV light (360 nm) prior to photoinduced orientation.

amorphous block of P3. This example illustrates the possible beneficial effects of transformation of the PS-*b*-PAzPy diblock copolymer by introducing the liquid crystallinity through H bonding.

3. Photoactive and Electroactive Diblock Copolymers. The PS-*b*-PAzPy diblock copolymer can also become both photoactive and electroactive through complexation between the PAzPy block and a metal-containing porphyrin such as zinc−tetraphenylporphyrin (ZnTPP). Figure 13 shows the UV−vis spectra in the solid state of pure ZnTPP and its complexes with the three diblock copolymers in Table 1. The molar ratio of ZnTPP to azopyridine was about 0.6. In the complexes, ZnTPP displays the dominant absorption around 435 nm, while the absorption of *trans*-azopyridine appears as a band near 355 nm. In all cases, the complexation via the axial coordination between N and Zn (Figure 1) is indicated by the characteristic red shift, by about 13 nm, of the β (554 nm) and α band (593 nm) of ZnTPP as well as the increased absorbance of the α band relative to the β band.[15] The linking of ZnTPP to the azopyridine moiety gives no LC phases but increases considerably T_g of the amorphous PAzPy block, as can be seen from the DSC heating curves of P2 and P3 complexed with ZnTPP in Figure 14. In contrast with pure P2 and P3 for which the glass transition of the PAzPy block can be noticed in the vicinity of 40 °C (Figure 4), the PAzPy block complexed with ZnTPP shows a higher T_g that apparently overlaps with T_g of the PS block. Using the homopolymer of PAzPy, it was found that T_g rises rapidly with the content of ZnTPP. The increase in T_g can be as much as 30 °C with only 25% of azopyridine complexed with ZnTPP. The bulky ZnTPP attached to the side chain of PAzPy appears to increase the rigidity of the polymer resulting in the increase of T_g. The difference in T_g between P2/ZnTPP

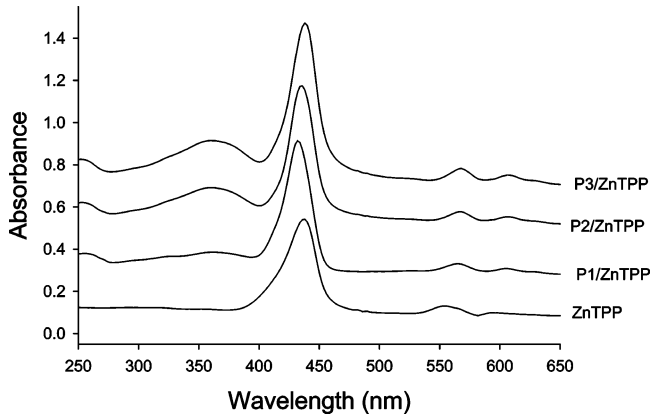

Figure 13. UV−vis spectra of thin films of ZnTPP and ZnTPP complexed with three diblock copolymers (P1−P3 samples).

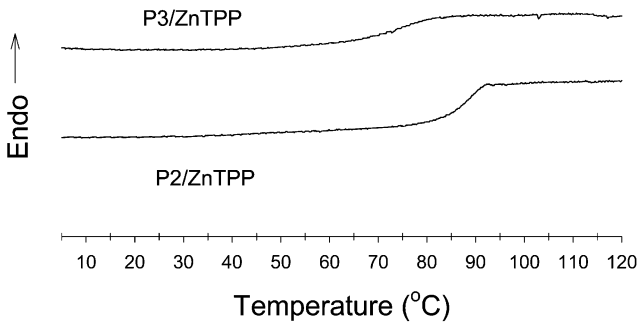

Figure 14. DSC heating curves (second scan) of two diblock copolymers (P2 and P3 samples) complexed with ZnTPP.

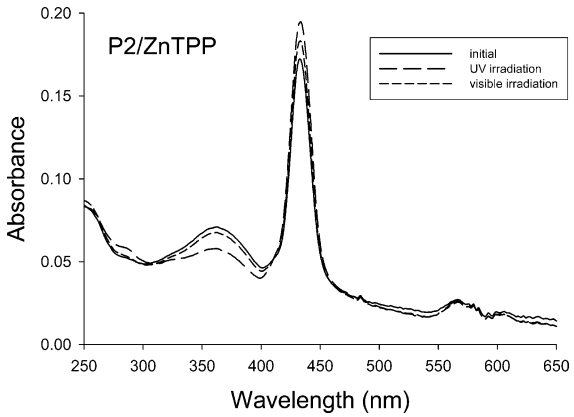

Figure 15. UV−vis spectra of a thin film of P2/ZnTPP showing the reversible trans−cis photoisomerization of azopyridine complexed with ZnTPP on UV and visible light irradiation.

and P3/ZnTPP may be a reflection of possible effects of the morphology of PAzPy microdomains on the increase in chain rigidity of ZnTPP complexed PAzPy.

The reversible photoisomerization of azopyridine moieties complexed with ZnTPP is shown in Figure 15. After a thin film of P2/ZnTPP was exposed to UV light (360 nm, 5 min), the absorption of *trans*-azopyridine at 355 nm decreased as a result of the trans−cis isomerization. The increase in the absorption of cis isomer around 450 nm (n−π* transition) is not discernible due to the overlap with the dominant absorption peak of porphyrin. Following visible light irradiation (440 nm, 5 min), the recovery of the population of *trans*-azopyridine can be noticed from the increase in the absorption of the trans isomer. On the other hand, it can be seen that the trans−cis photoisomerization of azopyridine is not very prominent, which may be caused by the bulky ZnTPP restricting the conformational change of the chromophore. During the cycle of trans−cis−trans isomerization of azopyridine, the absorptions of ZnTPP remain essentially unchanged, indicating that the photoisomerization of azopyridine does not or affect little the electronic transitions of ZnTPP.

In addition to the photoactivity retained after the complexation, the attachment of ZnTPP to azopyridine made the diblock copolymer become electroactive, too. Their electrochemical behavior in solution and in the solid state (thin film) was investigated. Figure 16 compares the cyclic voltammetry of P3/ZnTPP with neat ZnTPP and PAzPy/ZnTPP dissolved in an acetonitrile solution with 0.1 M TBAP. While neat ZnTPP displays its characteristic two states of oxidation/reduction,[16] the complexation with both the homopolymer PAzPy and the PAzPy block of P3 changed its redox behavior. The

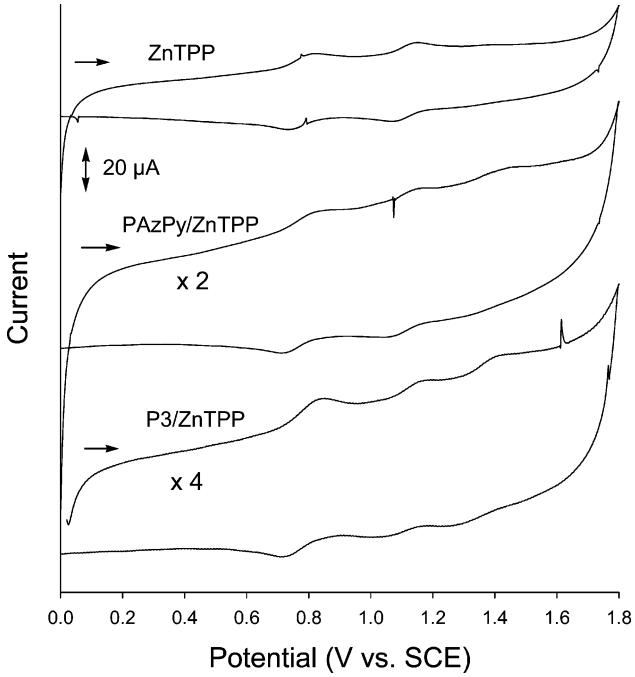

Figure 16. Cyclic voltammetry in solution for ZnTPP, PAzPy/ZnTPP, and P3/ZnTPP (acetonitrile/CH_2Cl_2, 0.1 M tetrabutylammonium perchlorate, SCE as reference electrolyte with a scanning rate of 100 mV/s). Data for PAzPy/ZnTPP and P3/ZnTPP are scaled by a factor of 2 and 4, respectively.

main difference is the appearance of a third oxidation peak at higher potential (~1.4 V) for the complexes of P3/ZnTPP and PAzPy/ZnTPP. This new redox state may arise from ZnTPP coordinated to azopyridine moieties. The possible dynamic equilibrium for the complexation reaction in solution means that part of ZnTPP would behave like they were alone. But even for unattached ZnTPP molecules, they were in a polymer solution, which may explain the slight shifts of the two redox states at lower potentials as compared with neat ZnTPP. In solution, the three pairs of redox peaks are visible for the complexes. Similar results were obtained for P2/ZnTPP. Note that either diblock copolymers or PAzPy uncomplexed with ZnTPP displayed no redox peaks under used conditions, which indicates that the third redox state is not due to the azopyridine moiety.

Some results of the cyclic voltammetry measurement on thin films are shown in Figure 17. In the solid state, the differences between neat ZnTPP and ZnTPP coordinated to the PAzPy are more pronounced. The two oxidation processes, corresponding to the formation of radical cation and dication of porphyrin, are shifted to higher potentials, particularly for the second process, for ZnTPP complexed with PAzPy. The effect of the length of the PAzPy block on the redox behavior of ZnTPP can be noticed from the second oxidation potential. With the homopolymer PAzPy it is shifted to about 1.49 V; with P3, which is the diblock copolymer having the highest content of PAzPy, it continues to increase slightly (~1.52 V). However, this oxidation peak appears to be suppressed for P2/ZnTPP. In the latter case, the apparent absence of the second oxidation suggests either a high potential outside the potential range used for the experiment or some sort of saturation of perchlorate anions (ClO_4^-) inside microdomains after the first oxidation process. Moreover, when the redox process was reversed, only a small reduction peak corresponding to the second oxidation process was noticeable for the

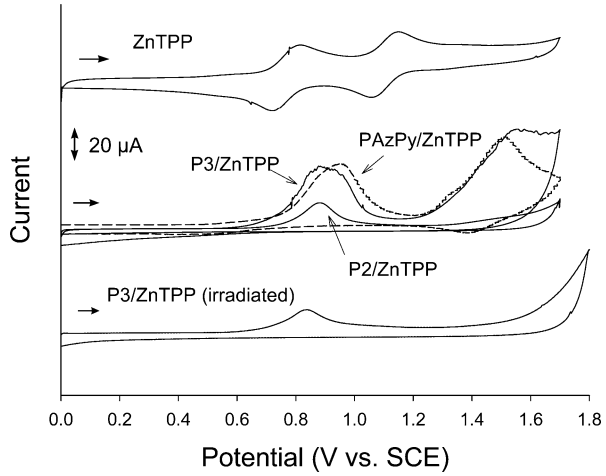

Figure 17. Cyclic voltammetry in the solid state for ZnTPP, PAzPy/ZnTPP (dashed line), P2/ZnTPP, P3/ZnTPP, and P3/ZnTPP subjected to UV light irradiation prior to the measurement (acetonitrile, 0.1 M tetrabutylammonium perchlorate, SCE as reference electrolyte with a scanning rate of 100 mV/s).

PAzPy/ZnTPP complex, while reduction peaks are totally absent for ZnTPP complexed with the two diblock copolymer samples, suggesting that perchlorate anions moving into the film during the oxidation process could not be released from the film when the potential was down. These results show that in the solid state the microdomain morphology of diblock copolymers may have even stronger effects than the homopolymer on the electrochemical behavior of ZnTPP. This is understandable because charge transfer through either spherical or cylindrical or lamellar microdomains of PAzPy should be hampered by PS matrix or lamella. For the complexes, no reduction peaks were observed even with a slow scanning rate of 5 mV/min.

Another intriguing observation is also shown in Figure 17. When the P3/ZnTPP film was irradiated with UV light (365 nm, 3 min) prior to the CV measurement, the photoisomerization of azopyridine appeared to affect the redox behavior of ZnTPP. The UV light irradiation made the first oxidation potential slightly reduced and eliminated completely the second oxidation peak. At this point, the mechanisms of the effects of the microphase-separated structure of the diblock copolymer and of the photoisomerization of azopyridine on the redox behavior of ZnTPP are unclear, and detailed investigations are outside the scope of this paper. Nevertheless, the interest revealed in this part of work is significant. Not only the use of coordination interaction between azopyridine and ZnTPP can render the PAzPy block both photoactive and electroactive, but also the effective loading of a redox-active molecule such as ZnTPP in microdomains of one building block points to the potential of exploring the self-assembly approach to prepare block copolymers with new functionalities. For instance, some metal−porphyrine-based compounds are used in photodynamic therapy for cancer treatment. It is conceivable that through self-assembly they can be complexed with the hydrophobic block of an amphiphilic block copolymer and thus loaded into polymer micelles used for drug delivery.

Conclusions

We report the synthesis, using ATRP, of the first diblock copolymer containing an azopyridine side-chain polymer and demonstrate the efficacy of using self-assembly through azopyridine to prepare multifunctional block copolymers. On one hand, we showed that linking a carboxylic acid, either aliphatic or aromatic or chiral, to azopyridine through H bonding can transform the amorphous PS-*b*-PAzPy diblock into a photoactive and LC diblock copolymer. The LC phase behavior of the PAzPy block is determined by the nature of the acid used, and the self-assembly-induced liquid crystallinity can improve significantly the photoinduced orientation of azobenzene mesogens inside the microdomains of PAzPy. On the other hand, we showed that metal-containing porphyrins such as ZnTPP can be complexed with azopyridine through coordination between the pyridyl group and metal, which makes the diblock copolymer both photoactive and electroactive. The redox behavior of ZnTPP linked to PAzPy is affected by the microdomain morphology and also appears to be influenced by the photoisomerization of azopyridine. This part of work showed that self-assembly using azopyridine-containing block copolymers is an effective way to load metal−porphyrins inside self-organized microdomains of block copolymers, which promises interest for possible applications.

Acknowledgment. The authors thank Prof. Andrzej Lasia, Dr. Rafal Jurczakowski, and Mr. Mihai Ciprian Cirtiu for cyclic voltammetry measurements and helpful discussions as well as Mrs. Patricia Basque and Rodica Plesu (Laval University) for X-ray scattering measurements. They are also grateful to Natural Sciences and Engineering Research Council of Canada and le Fonds québécois de la recherche sur la nature et les technologies of Québec for their financial support.

References and Notes

(1) Chao, C.-Y.; Li, X.; Ober, C.; Osuji, C.; Thomas, E. *Adv. Funct. Mater.* **2004**, *4*, 364.
(2) Cui, L.; Zhao, Y.; Yavrian, A.; Galstian, T. *Macromolecules* **2003**, *36*, 8246.
(3) Tong, X.; Cui, L.; Zhao, Y. *Macromolecules* **2004**, *37*, 3101.
(4) Cui, L.; Tong, X.; Yan, X.; Liu, G.; Zhao, Y. *Macromolecules* **2004**, *37*, 7097.
(5) Wang, G.; Tong, X.; Zhao, Y. *Macromolecules* **2004**, *37*, 8911.
(6) Cui, L.; Zhao, Y. *Chem. Mater.* **2004**, *16*, 2076.
(7) Lacey, D.; Beattie, H. N.; Mitchell, G. R.; Pople, J. A. *J. Mater. Chem.* **1998**, *8*, 53.
(8) Ciampolinim, M.; Nardi, N. *Inorg. Chem.* **1966**, *5*, 41.
(9) Xia, J.; Zhang, X.; Matyjaszewski, K. *Macromolecules* **1999**, *32*, 3531.
(10) Cui, L.; Lattermann, G. *Macromol. Chem. Phys.* **2002**, *203*, 2432.
(11) Zhu, L.; Cheng, S. Z. D.; Calhoun, B. H.; Ge, Q.; Quirk, R. P.; Thomas, E. L.; Hsiao, B. S.; Yeh, F.; Lotz, B. *Polymer* **2001**, *42*, 5829.
(12) (a) Kato, T.; Frechet, J. M. J. *Macromolecules* **1989**, *22*, 3818. (b) Kato, T.; Kihara, H.; Uryu, T.; Fujishima, A.; Frechet, J. M. J. *Macromolecules* **1992**, *25*, 6836. (c) Kumar, U.; Kato, T.; Frechet, J. M. J. *J. Am. Chem. Soc.* **1992**, *114*, 6630.
(13) Lee, J. Y.; Painter, P. C.; Coleman, M. M. *Macromolecules* **1988**, *21*, 954.
(14) Kato, T.; Frechet, J. M. J.; Wilson, P. G.; Saito, T.; Uryu, T.; Fujishima, A.; Jin, C.; Kaneuchi, F. *Chem. Mater.* **1993**, *5*, 1094.
(15) D'Souza, F.; Hsieh, Y.-Y.; Deviprasad, G. R. *Inorg. Chem.* **1996**, *15*, 5747.
(16) Kadish, K. M.; Shiue, L. R.; Rhodes, R. K.; Bottomley, L. A. *Inorg. Chem.* **1981**, *20*, 1274.

MA047364M